

Dongdong Wang · Jiun-Shyan Chen

A locking-free meshfree curved beam formulation with the stabilized conforming nodal integration

Received: 22 July 2005 / Accepted: 22 September 2005
© Springer-Verlag 2005

Abstract A locking-free meshfree curved beam formulation based on the stabilized conforming nodal integration is presented. Motivated by the pure bending solutions of thin curved beam, a meshfree approximation is constructed to represent pure bending mode without producing parasitic shear and membrane deformations. Furthermore, to obtain the exact pure bending solution (bending exactness condition), the integration constraints corresponding to the Galerkin weak form are derived. A nodal integration with curvature smoothing stabilization that satisfies the integration constraints is proposed under the Galerkin weak form for shear deformable beam. Numerical examples demonstrate that the resulting meshfree formulation can exactly reproduce pure bending mode with arbitrary discretizations, and the method is stable and free of shear and membrane locking. Computational efficiency and accuracy are achieved simultaneously in the proposed formulation.

Keywords Meshfree method · Curved beam · Shear and membrane locking · Stabilized conforming nodal integration

1 Introduction

Due to the flexibility in constructing approximation functions with desired smoothness and accuracy, meshfree methods have been successfully applied to Kirchhoff type of plate and shell problems where the C^1 continuity of approximation is required [9, 10]. For Mindlin–Reissner plate problem, employing approximation function for rotational degrees of

freedom as the derivatives of the approximation function for translational degrees of freedom has been introduced to eliminate shear locking [6, 8]. Higher order basis functions have been employed in h-p cloud method to relieve the shear locking [7].

Locking can also be relieved by using a nodal integration, however this often leads to the rank deficiency type of spatial instability [2, 4, 5]. A stabilized conforming nodal integration (SCNI) has been proposed to stabilize the nodal integration [4, 5] of meshfree Galerkin weak form. Along this route, a locking free SCNI for meshfree Mindlin–Reissner plate formulation has been proposed [14, 15]. In this approach, the reproducibility of Kirchhoff mode, termed Kirchhoff mode reproducing conditions (KMRC), was identified for Mindlin–Reissner plate problem, and thus meshfree approximations of displacements and rotations were constructed to meet KMRC. In addition, the integration constraints for achieving bending exactness (BE) were derived, and a curvature smoothing has been proposed to meet bending integration constraints and to provide stability to the nodally integrated weak form. This approach is also free of locking in the limit of thin plate.

In this study, the previous methodology is extended to shear deformable curved beam problems where the membrane and shear locking need to be taken into account. The KMRC for curved beam is first studied and as a result a meshfree approximation which meets KMRC is proposed. This approximation leads to zero parasitic membrane and shear deformation under pure bending. Moreover, the corresponding integration constraints for bending exactness are derived, and a curvature smoothing is introduced to satisfy these constraints. This paper is organized as follows. The governing equations of curved beam are briefed in Sect. 2. In Sect. 3 the meshfree integration constraints for curved beam under pure bending are derived, and meshfree shape functions that meet KMRC are presented. Then curvature smoothing stabilization and the resulting discrete meshfree equations are discussed in Sect. 4. Finally numerical examples and concluding remarks are presented in Sect. 5 and 6, respectively.

D. Wang (✉)
Department of Civil Engineering,
Xiamen University, Xiamen,
Fujian, 361005, P.R. China
E-mail: ddwang@xmu.edu.cn,
Fax: +86-592-2186421

J.-S. Chen
Department of Civil and Environmental Engineering,
University of California, Los Angeles,
CA 90095-1593, USA

2 Governing equations of curved beam

2.1 Kinematics and weak form

Consider a curved beam as shown in Fig. 1, where R is the radius, s is the curvilinear axial coordinate along the axis of curved beam, and t is the thickness. The beam occupies a domain $\Omega = (0, L)$, i.e., $s \in (0, L)$, with boundary $\partial\Omega = \{s = 0 \text{ or } s = L\}$. To describe the first order shear deformation theory, we define notations as follows: (1) displacement variables: two middle surface displacements and one bending rotation $\{u(s), v(s), \theta(s)\}$; (2) deformation measures: membrane strain, shear strain, and curvature $\{\varepsilon(s), \gamma(s), \kappa(s)\}$; and (3) normal force, shear force, and couple resultants $\{N(s), V(s), M(s)\}$. The sign convention of displacements is shown in Fig. 1. The signs of the three resultants are consistent with their corresponding kinematic measures.

The strain measures are obtained from the kinematic variables as follows:

$$\varepsilon(s) = \frac{du(s)}{ds} + \frac{v(s)}{R}, \quad (1)$$

$$\gamma(s) = \frac{\partial v(s)}{\partial s} - \theta(s) - \frac{u(s)}{R}, \quad (2)$$

$$\kappa(s) = \frac{d\theta(s)}{ds}. \quad (3)$$

The constitutive relations are

$$\begin{Bmatrix} N(s) \\ M(s) \\ V(s) \end{Bmatrix} = \begin{bmatrix} EA & 0 & 0 \\ 0 & EI & 0 \\ 0 & 0 & kGA \end{bmatrix} \begin{Bmatrix} \varepsilon(s) \\ \kappa(s) \\ \gamma(s) \end{Bmatrix} \quad (4)$$

where E , G , A , I are the Young's modulus, shear modulus, area of cross section, and moment of inertia, respectively, k is the shear correction factor, and $k = 5/6$ for a rectangular cross section.

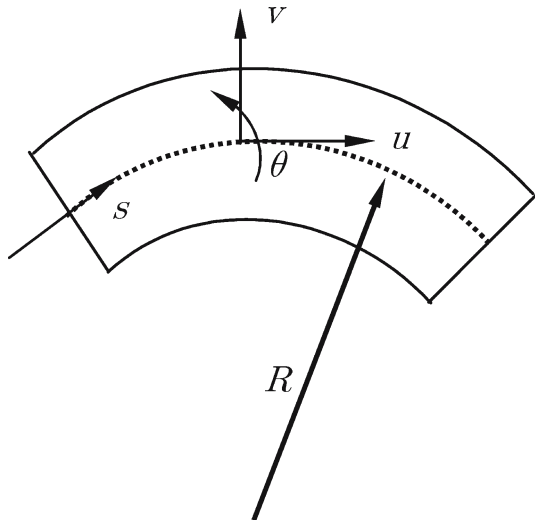


Fig. 1 Kinematics of a curved beam

The weak form of a shear deformable curved beam can be stated as

$$\int_0^L \delta\kappa EI \kappa ds + \int_0^L \delta\varepsilon EA \varepsilon ds + \int_0^L \delta\gamma kGA \gamma ds - \delta W^{\text{ext}} = 0 \quad (5)$$

with

$$\begin{aligned} \delta W^{\text{ext}} = & \int_0^L \delta u n(s) ds + \int_0^L \delta\theta m(s) ds \\ & + \int_0^L \delta v q(s) ds + \delta\Lambda, \end{aligned} \quad (6)$$

where $n(s)$, $q(s)$ and $m(s)$ denote the distributed circumferential, radial and moment loadings along the beam axis, respectively, and $\delta\Lambda$ represents the virtual work associated with point loads.

3 Bending exactness conditions

To avoid shear and membrane locking in the numerical solution of the variational equation in Sect. 2, we require the meshfree approximation be capable of representing pure bending modes, termed KMRC in [14, 15]. Using the Castigliano's theorem, the solutions of a thin curved beam under pure bending \bar{M} as shown in Fig. 2 are as follows:

$$\begin{aligned} u(s) &= \frac{\bar{M} R^2}{EI} \left(\sin\left(\frac{s}{R}\right) - \frac{s}{R} \right), \\ v(s) &= \frac{\bar{M} R^2}{EI} \left(1 - \cos\left(\frac{s}{R}\right) \right), \\ \theta(s) &= \frac{\bar{M} s}{EI}. \end{aligned} \quad (7)$$

In this section, the moving least-square/reproducing kernel (MLS/RK) approximation [3, 11] is introduced, and the necessary conditions to meet bending exactness in the numerical solution of the variational equation are presented.

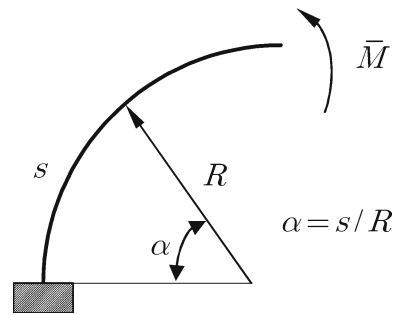


Fig. 2 A curved beam under pure bending

3.1 MLS/RK approximation

Here we define the MLS/RK approximation using the curvilinear coordinate s . Let the beam domain be discretized by NP nodes s_I , $I = 1, 2, \dots, NP$. The MLS/RK approximation of a field variable $u(s)$, denoted by $u^h(s)$, can be expressed as:

$$u^h(s) = \sum_{I=1}^{NP} \Psi_I(s) d_I, \quad (8)$$

where d_I is the generalized nodal coefficient and $\Psi_I(s)$ is the meshfree shape function given by

$$\Psi_I(s) = \mathbf{h}^T(s_I) \mathbf{b}(s) \phi(s - s_I), \quad (9)$$

where $\phi(s - s_I)$ is the kernel function centered at s_I with a compact support, and $\mathbf{h}(s) = \{h_0(s), h_1(s), h_2(s), \dots, h_n(s)\}^T$ is the vector containing basis functions $h_i(s)$, $\mathbf{b}(s) = \{b_0(s), b_1(s), b_2(s), \dots, b_n(s)\}^T$ is the coefficient vector solved by imposing the following n -th order reproducing conditions

$$\sum_{I=1}^{NP} \Psi_I(s) h_i(s_I) = h_i(s) \quad 0 \leq i \leq n. \quad (10)$$

Substituting Eq. (9) into Eq. (10) gives

$$\mathcal{M}(s) \mathbf{b}(s) = \mathbf{h}(s) \quad (11)$$

with \mathcal{M} being the moment matrix given by

$$\mathcal{M}(s) = \sum_{I=1}^{NP} \mathbf{h}(s_I) \mathbf{h}^T(s_I) \phi(s - s_I). \quad (12)$$

Thus we have $\mathbf{b}(s) = \mathcal{M}^{-1}(s) \mathbf{h}(s)$, and the meshfree shape function is obtained as

$$\Psi_I(s) = \mathbf{h}^T(s_I) \mathcal{M}^{-1}(s) \mathbf{h}(s) \phi(s - s_I). \quad (13)$$

Not that this MLS/RK approximation of Eq. (13) reproduces any basis function $h_i(s)$. When the polynomial bases are used, i.e., $h_i(s) = s^i$, one can show the followings for shifted basis

$$\sum_{I=1}^{NP} \Psi_I(s) h_i(s - s_I) = \delta_{i0} \quad (14)$$

$$\text{or } \sum_{I=1}^{NP} \Psi_I(s) (s - s_I)^i = \delta_{i0} \quad 0 \leq i \leq n, \quad (14)$$

and the shape function takes the following form:

$$\Psi_I(s) = \mathbf{h}^T(0) \mathcal{M}^{-1}(s) \mathbf{h}(s - s_I) \phi(s - s_I), \quad (15)$$

where

$$\mathcal{M}(s) = \sum_{I=1}^{NP} \mathbf{h}(s - s_I) \mathbf{h}^T(s - s_I) \phi(s - s_I), \quad (16)$$

$$\mathbf{h}^T(s - s_I) = \{1, s - s_I, \dots, (s - s_I)^n\}^T. \quad (17)$$

Although Eqs. (13) and (15) are mathematically equivalent, the shifting basis gives the moment matrix a better conditioning number. Note that if the basis function is not polynomial bases, the shifted form in Eq. (15) generally cannot be obtained.

3.2 Kirchhoff mode reproducing condition in curved beam

Kirchhoff mode reproducing condition requires that the numerical shear and membrane strains vanish for a beam under pure bending. In the MLS/RK approximation of displacements, we have

$$\begin{aligned} \begin{Bmatrix} u^h(s) \\ v^h(s) \\ \theta^h(s) \end{Bmatrix} &= \sum_I \begin{bmatrix} \Psi_I(s) & 0 & 0 \\ 0 & \Psi_I(s) & 0 \\ 0 & 0 & \Psi_I(s) \end{bmatrix} \begin{Bmatrix} u_I \\ v_I \\ \theta_I \end{Bmatrix} \\ &\equiv \sum_I \Psi_I(s) \mathbf{d}_I. \end{aligned} \quad (18)$$

Consequently, the membrane strain ε , shear strain γ , and curvature κ are approximated as:

$$\varepsilon^h(s) = u_{,s}^h(s) + \frac{v^h(s)}{R} \equiv \sum_I \mathbf{B}_I^m(s) \mathbf{d}_I, \quad (19)$$

$$\gamma^h(s) = v_{,s}^h(s) - \theta^h(s) - \frac{u^h(s)}{R} \equiv \sum_I \mathbf{B}_I^s(s) \mathbf{d}_I, \quad (20)$$

$$\kappa^h(s) = \theta_{,s}^h(s) \equiv \sum_I \mathbf{B}_I^b(s) \mathbf{d}_I, \quad (21)$$

where

$$\mathbf{B}_I^m(s) = \left\{ \Psi_{I,s}(s) \frac{\Psi_I(s)}{R} \ 0 \right\}, \quad (22)$$

$$\mathbf{B}_I^s(s) = \left\{ -\frac{\Psi_{I,s}(s)}{R} \ \Psi_{I,s}(s) - \Psi_I(s) \right\}, \quad (23)$$

$$\mathbf{B}_I^b(s) = \{ 0 \ 0 \ \Psi_{I,s}(s) \}, \quad (24)$$

$$\mathbf{d}_I = \{ u_I \ v_I \ \theta_I \}^T. \quad (25)$$

Let \mathbf{d}_I^b denote the coefficient vector associated with a pure bending deformation corresponding to Eq. (7)

$$\mathbf{d}_I^b = \begin{Bmatrix} \frac{\bar{M} R^2}{EI} \left(\sin\left(\frac{s_I}{R}\right) - \frac{s_I}{R} \right) \\ \frac{\bar{M} R^2}{EI} \left(1 - \cos\left(\frac{s_I}{R}\right) \right) \\ \frac{\bar{M} s_I}{EI} \end{Bmatrix}. \quad (26)$$

To reproduce the pure bending mode in the approximation, we need

$$\begin{aligned} \sum_I \mathbf{B}_I^m \mathbf{d}_I^b &= 0, \\ \sum_I \mathbf{B}_I^s \mathbf{d}_I^b &= 0, \\ \sum_I \mathbf{B}_I^b \mathbf{d}_I^b &= \bar{M} = \text{constant}. \end{aligned} \quad (27)$$

Substituting Eq. (26) into Eq. (27) yields

$$\sum_I \Psi_{I,s} R \cos\left(\frac{s_I}{R}\right) + \sum_I \Psi_I \sin\left(\frac{s_I}{R}\right) = 0, \quad (28)$$

$$\sum_I \Psi_{I,s} R \sin\left(\frac{s_I}{R}\right) - \sum_I \Psi_I \cos\left(\frac{s_I}{R}\right) = 0, \quad (29)$$

$$\sum_I \Psi_I = 1; \sum_I \Psi_I s_I = s; \sum_I \Psi_I s_I^2 = 1. \quad (30)$$

The above pure bending conditions can be met if the following reproducing conditions hold in the MLS/RK shape functions:

$$\sum_I \Psi_I \cos\left(\frac{s_I}{R}\right) = \cos\left(\frac{s}{R}\right), \quad (31)$$

$$\sum_I \Psi_I \sin\left(\frac{s_I}{R}\right) = \sin\left(\frac{s}{R}\right), \quad (32)$$

$$\sum_I \Psi_I s_I^i = s^i, \quad i = 0, 1. \quad (33)$$

The above conditions can be satisfied by selecting the following basis functions in the MLS/RK approximation:

$$\mathbf{h}^T(s) = \left\{ 1 \quad s \sin\left(\frac{s}{R}\right) \cos\left(\frac{s}{R}\right) \right\}. \quad (34)$$

Note that since MLS/RK is a local approximation, the radius of curvature R in Eq. (34) is allowed to vary in the problem domain, i.e., $R = R(s)$.

3.3 Integration constraints

To pass pure bending test under Galerkin framework, we employ basis functions of Eq. (34) in the MLS/RK approximation, and the next task is to investigate the integration requirement in the domain integration of the weak form. The integration constraints are identified by enforcing the pure bending mode to satisfy the discrete equilibrium equation corresponding to the weak form of curved beam. Introducing the pure bending nodal vector d_I^b of Eq. (26) into the weak form of Eq. (5), and with the consideration that MLS/RK approximation using the basis functions in Eq. (34) to meet the pure bending reproducing conditions in Eq. (27), yields the following reduced weak form:

$$\int_0^L \delta \kappa^h EI \kappa^h ds = \delta \theta^h(s_{NP}) \bar{M}, \quad (35)$$

where without loss of generality the bending moment \bar{M} is applied at the end of the beam $s = L$, and s_{NP} denotes this boundary point. The corresponding discrete equation is

$$\int_0^L (\mathbf{B}_I^b)^T EI \mathbf{B}^b \mathbf{d}^b ds = N_I^T(s_{NP}) \bar{M};$$

$$\mathbf{N}_I(s) = \{0 \ 0 \ \Psi_I(s)\}. \quad (36)$$

Recall Eq. (27), we have $M = EI \mathbf{B}^b \mathbf{d}^b = \bar{M}$, and thus

$$\int_0^L (\mathbf{B}_I^b)^T \bar{M} ds = \int_0^L (\mathbf{B}_I^b)^T ds \bar{M}. \quad (37)$$

Since \bar{M} is an arbitrary constant, the discrete equilibrium equation (37) leads to

$$\int_0^L (\mathbf{B}_I^b)^T ds = \mathbf{N}_I^T(s_{NP}). \quad (38)$$

Thus, the integration constraints for exact bending solution are

$$\sum_{K=1}^{N_{\text{int}}} \mathbf{B}_I^b(s_K) w_K = \mathbf{0} \text{ for nodes } \{I \mid \text{supp}(\Psi_I) \cap s_{NP} = \emptyset\}, \quad (39)$$

$$\sum_{K=1}^{N_{\text{int}}} \mathbf{B}_J^b(s_K) w_K = N_J(s_{NP}) \text{ for nodes } \{J \mid \text{supp}(\Psi_J) \cap s_{NP} \neq \emptyset\}, \quad (40)$$

where N_{int} is the total number of integration points for domain integration, s_K is the domain integration point, and w_K is the corresponding integration weight.

4 Curvature smoothing in nodal integration of curved beam

A nodal integration is developed here to fulfill bending exactness and integration constraints of Eqs. (39) and (40), as well as to remove rank deficiency in the nodally integrated weak form. To start, introduce the following curvature smoothing at nodal point s_K :

$$\begin{aligned} \tilde{\kappa}(s_K) &= \frac{1}{L_K} \int_{\Omega_K} \kappa(s) ds = \frac{1}{L_K} \int_{\Omega_K} \theta_{,s} ds \\ &= [\theta(s_K^+) - \theta(s_K^-)] / L_K, \end{aligned} \quad (41)$$

where L_K is the length of nodal representative domain $\Omega_K = (s_K^-, s_K^+)$, and s_K^- and s_K^+ can be defined as the middle points between s_{K-1} and s_K , s_K and s_{K+1} , respectively. Introducing the MLS/RK approximation of θ in Eq. (18) into Eq. (41) gives

$$\tilde{\kappa}^h(s_K) = \sum_{I=1}^{NP} \tilde{\mathbf{B}}_I^b(s_K) \mathbf{d}_I, \quad (42)$$

$$\tilde{\mathbf{B}}_I^b(s_K) = \{0 \ 0 \ \tilde{\nabla} \Psi_I(s_K)\}, \quad (43)$$

$$\tilde{\nabla} \Psi_I(s_K) = [\Psi_I(s_K^+) - \Psi_I(s_K^-)] / L_K. \quad (44)$$

Following the derivation in [4,5,15], it is straightforward to show that the integration constraints in Eqs. (39) and (40) are satisfied exactly.

Based on the assumed strain method [13], the smoothed curvature and the MLS/RK approximation are introduced into the nodally integrated weak form as follows

$$\begin{aligned}
& \sum_{K=1}^{NP} [\delta \tilde{\kappa}^{hT}(s_K) E I \tilde{\kappa}^h(s_K) + \delta \gamma^{hT}(s_K) k G A \gamma^h(s_K) \\
& \quad + \delta \varepsilon^{hT}(s_K) E A \varepsilon^h(s_K)] L_K \\
& = \sum_{K=1}^{NP} [\delta u^h(s_K) n(s_K) + \delta v^h(s_K) q(s_K) \\
& \quad + \delta v^h(s_K) m(s_K)] L_K \\
& \quad + \delta u^{hT}(s_{NP}) \bar{N} + \delta v^{hT}(s_{NP}) \bar{V} + \delta \theta^{hT}(s_{NP}) \bar{M}
\end{aligned} \quad (45)$$

with

$$\begin{aligned}
\tilde{\kappa}^h(s_K) &= \sum_{I=1}^{NP} \tilde{\mathbf{B}}_I^b(s_K) \mathbf{d}_I; \gamma^h(s_K) = \sum_{I=1}^{NP} \mathbf{B}_I^s(s_K) \mathbf{d}_I; \varepsilon^h(s_K) \\
&= \sum_{I=1}^{NP} \mathbf{B}_I^m(s_K) \mathbf{d}_I,
\end{aligned} \quad (46)$$

where s_K is nodal point coordinate, L_K is the nodal representative arc length used in the curvature smoothing, and $\tilde{\mathbf{B}}_I^b$, \mathbf{B}_I^s and \mathbf{B}_I^m are given in Eqs.(43), (22) and (23), respectively.

Finally the resulting discrete equation of curved beam is

$$\mathbf{K} \mathbf{d} = \mathbf{f}, \quad (47)$$

where

$$\mathbf{K} = \mathbf{K}^b + \mathbf{K}^s + \mathbf{K}^m, \quad (48)$$

$$\mathbf{K}_{IJ}^b = \sum_{K=1}^{NP} (\tilde{\mathbf{B}}_I^b)^T(s_K) E I \tilde{\mathbf{B}}_J^b(s_K) L_K, \quad (49)$$

$$\mathbf{K}_{IJ}^s = \sum_{K=1}^{NP} (\mathbf{B}_I^s)^T(s_K) k G A \mathbf{B}_J^s(s_K) L_K, \quad (50)$$

$$\mathbf{K}_{IJ}^m = \sum_{K=1}^{NP} (\mathbf{B}_I^m)^T(s_K) E A \mathbf{B}_J^m(s_K) L_K, \quad (51)$$

$$\mathbf{f}_I = \Psi_I(s_{NP}) \begin{pmatrix} \bar{N} \\ \bar{V} \\ \bar{M} \end{pmatrix} + \sum_{K=1}^{NP} \Psi_I(s_K) \begin{Bmatrix} n(s_K) \\ q(s_K) \\ m(s_K) \end{Bmatrix} L_K. \quad (52)$$

5 Numerical tests

5.1 Pure bending test for a clamped-free curved beam

The geometry and material properties of the curved beam as shown in Fig. 2 are: radius $R = 10$, cross section width $b = 1$ and height $t = 0.01$, Young's modulus $E = 2 \times 10^9$, and Poisson ratio $\nu = 0.3$. The beam is subjected to a unit moment at the end.

In the numerical test, a non-uniform 11 point discretization shown as solid circles in Fig. 3 is used. The errors

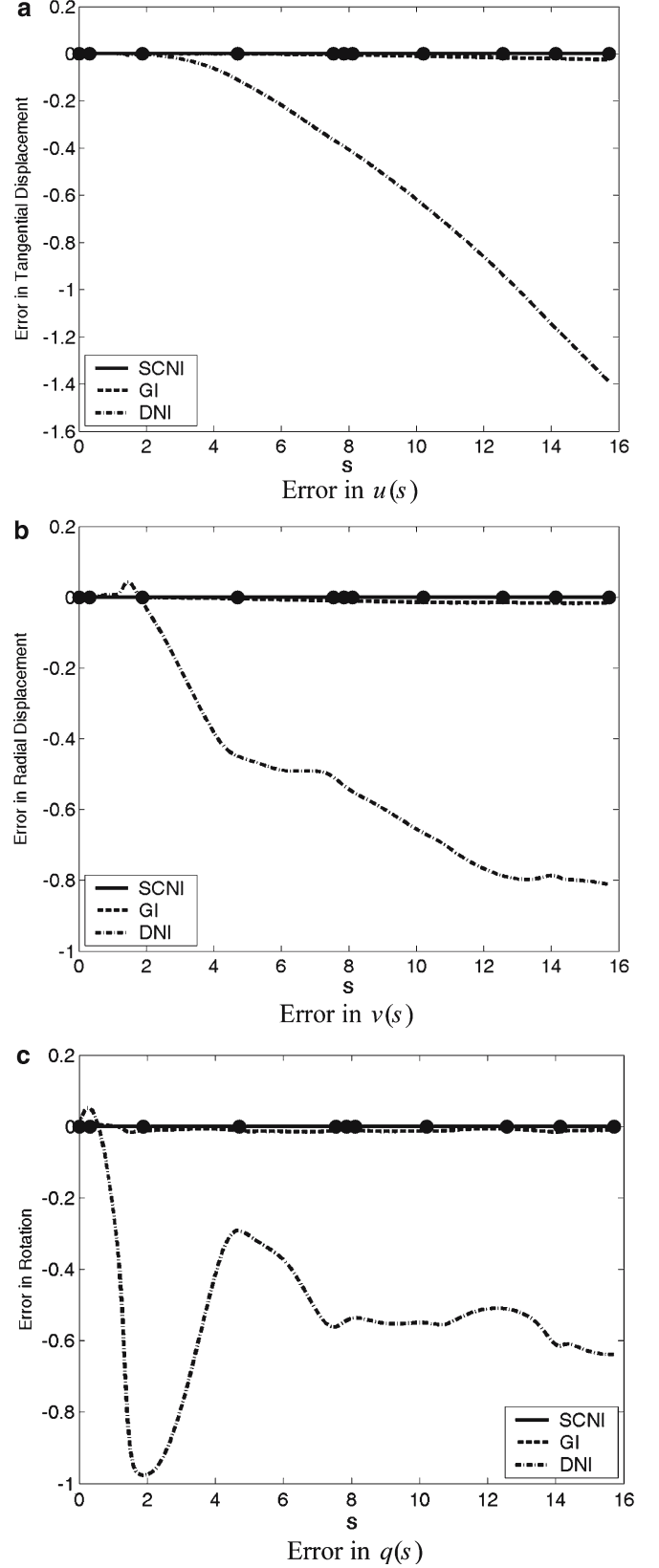


Fig. 3 Solution errors in the curved beam subjected to pure bending: **a** Error in $u(s)$; **b** Error in $v(s)$; **c** Error in $\theta(s)$

of numerical solutions are compared to the analytical solution. For comparison, direct nodal integration (DNI), Gauss integration (GI) with five-point quadrature rule, and SCNI discussed in Sect. 4 are employed. The normalized support size of kernel function in the MLS/RK approximation is set to be 3.1 through out this study. Here for irregular discretization, the normalized support size means the actual support size divided by the average nodal space between adjacent nodes. The numerical results for pure bending in Fig. 3 show an unstable solution in DNI. There is still noticeable error even for the GI with five-point quadrature rule. In contrast the proposed SCNI produces the exact solutions regardless of the discretization pattern.

5.2 Analysis of a pinched ring

As shown in Fig. 4, a ring is pinched by two opposite point loads P . The geometry and material properties are: radius $R = 4.953$, cross section width $b = 1$, Young's modulus $E = 1.05 \times 10^7$, and Poisson ratio $\nu = 0.3125$. Based on the Castiglano's energy theorem, the exact vertical tip displacement under the load is found as

$$v_P = -\frac{PR\pi}{8} \left[\frac{R^2}{EI} \left(1 - \frac{8}{\pi^2} \right) + \frac{1}{kGA} + \frac{1}{EA} \right]. \quad (53)$$

Due to the two-fold symmetry, only a quarter of the ring is modeled. Kernel function with normalized support size of 3.1 is used herein. Figure 5 shows a locking test using a six-node discretization for a quarter span, and the numerical solution of under-load deflection is normalized by the analytical solution of Eq. (53). The results show a significant locking in GI, whereas the proposed SCNI gives a locking-free solution. The L_2 error norms of moment obtained by using DNI, GI and SCNI for length to thickness ratio of 10^4 are shown in Fig. 6 where the label " h " of the horizontal axis denotes the nodal space between two neighboring nodes. The results demonstrate the superior convergence behavior

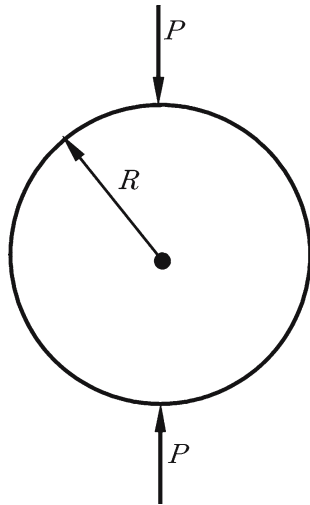


Fig. 4 Pinched ring

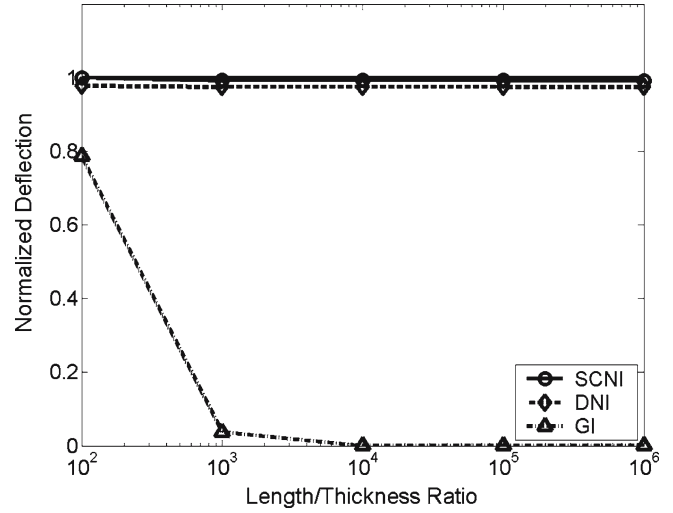


Fig. 5 Locking test for the pinched ring

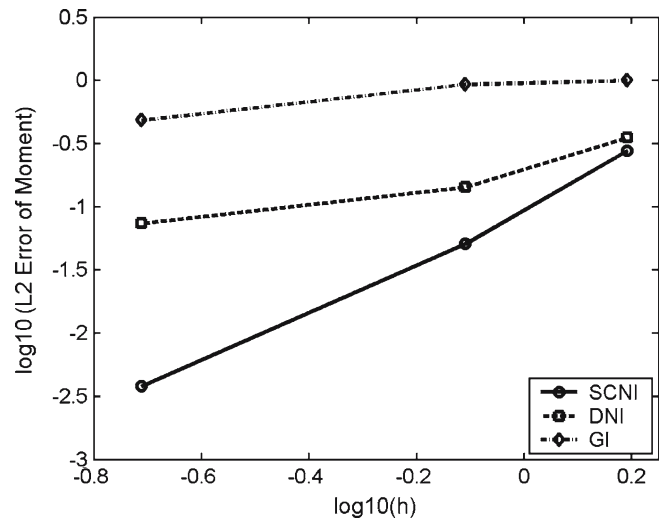


Fig. 6 L_2 error norm of moment for the pinched ring

of SCNI compared to GI and DNI. The moment distributions for a non-uniform 11 node discretization with a 3.5 normalized support are plotted in Fig. 7 (solid circles denote the nodal locations). The results show that SCNI solution is stable and most accurate compared with those of DNI and GI. The convergence of vertical displacement under the load using the proposed method for this problem with thickness $t = 0.094$ is shown in Fig. 8, where the SCNI meshfree solution is also compared favorably with the results of other well-known finite element curved beam formulations (CMCS [1], CL1 [12]).

5.3 Analysis of a nearly straight beam

A clamped-free beam with a relatively large radius/span ratio as shown in Fig. 9 is tested here to demonstrate the effectiveness of the proposed approach to approximate the straight

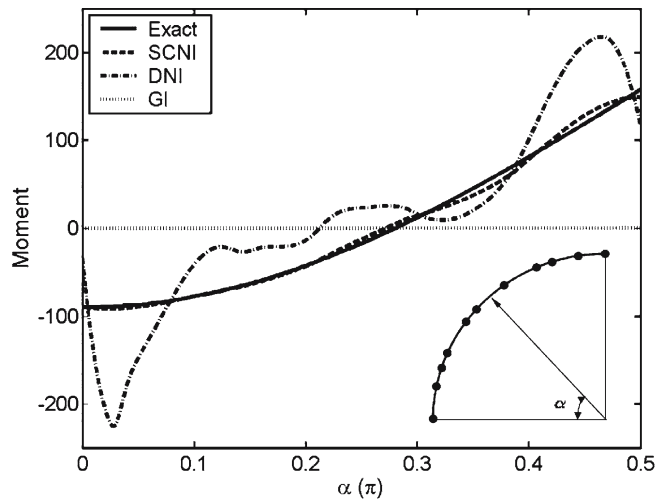


Fig. 7 Moment with irregular discretization for the pinched ring

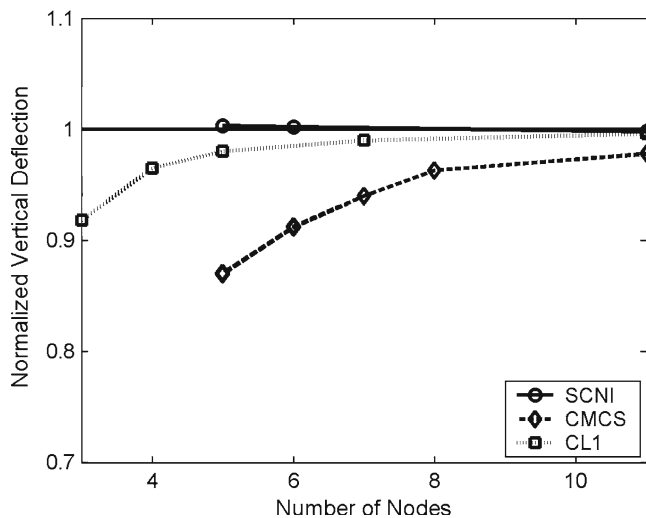


Fig. 8 Vertical displacement under the load for the pinched ring



Fig. 9 Clamped-free straight beam subjected to a tip load

beam configuration. The geometry and material properties are as follows: radius $R = 1000$, beam span $s = 10$, cross section width $b = 1$ and height $t = 0.01$, Young's modulus $E = 2 \times 10^9$, and Poisson ratio $\nu = 0.3$. A unit vertical concentrated load is applied at the right end. This beam is discretized only by five uniformly distributed nodes and kernel function with a normalized support size of 3.1 is employed. The results as shown in Figs. 10a and b demonstrate that the proposed formulation can approximate the straight beam very accurately.

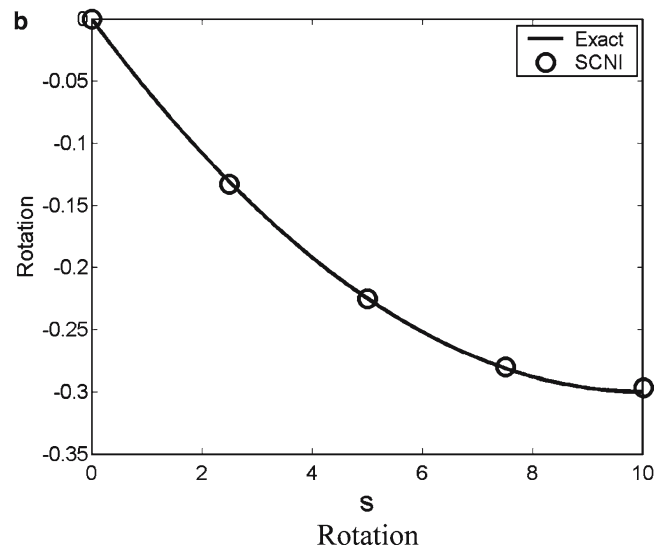
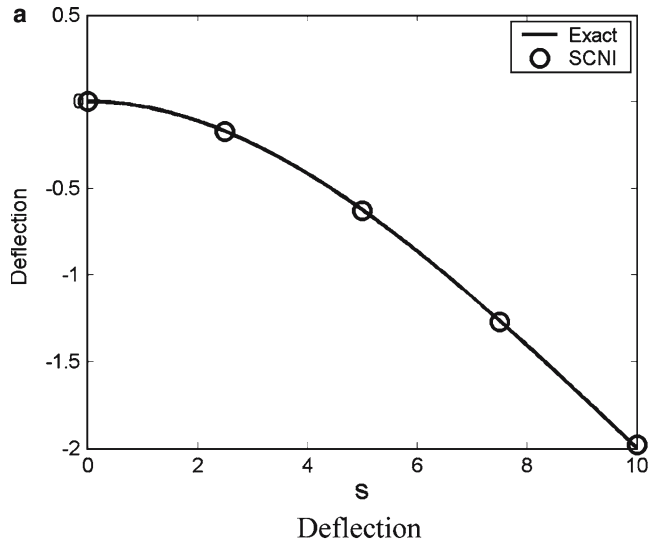


Fig. 10 Solutions for the clamped-free straight beam: a deflection; b rotation

6 Concluding remarks

A locking-free meshfree formulation based on the SCNI was presented to solve curved beam problems. The proposed method contains two major components: (1) construction of a MLS/RK approximation which is capable of representing pure bending mode of curved beam without producing parasitic shear and membrane deformations; (2) nodal integration of the Galerkin weak form with curvature smoothing stabilization to remove the rank deficiency in the nodally integrated stiffness matrix and to pass the pure bending test.

Numerical tests have shown that the proposed approach exactly reproduces pure bending mode for arbitrary discretization. On the other hand, it has been shown that the meshfree formulation using DNI produces unstable solutions, and the case with GI with 5-point quadrature rule yields less accurate results compared to the proposed method. The locking test

has demonstrated that the proposed approach is free of shear and membrane locking, whereas GI solution has a severe locking. The proposed SCNI approach also demonstrated superior convergence rates over those of GI and DNI. Both accuracy and efficiency are achieved in the proposed curved beam formulation.

Acknowledgements The support of this work by the Research Initiation Fund of Xiamen University to the first author is greatly acknowledged.

References

1. Babu CR, Prathap G (1986) A linear thick curved beam element. *Int J Numer Meth Eng* 23:1313–1328
2. Beissel S, Belytschko T (1996) Nodal integration of the element-free Galerkin method. *Comput Meth Appl Mech Eng* 139:49–74
3. Belytschko T, Lu YY, Gu L (1994) Element-free Galerkin methods. *Int J Numer Meth Eng* 37:229–256
4. Chen JS, Wu CT, Yoon S, You Y (2001) A stabilized conforming nodal integration for Galerkin meshfree methods. *Int J Numer Meth Eng* 50:435–466
5. Chen JS, Yoon S, Wu CT (2002) Nonlinear version of stabilized conforming nodal integration for Galerkin meshfree methods. *Int J Numer Meth Eng* 53:2587–2615
6. Donning B, Liu WK (1998) Meshless methods for shear-deformable beams and plates. *Comput Meth Appl Mech Eng* 152:47–72
7. Garcia O, Fancello EA, Barcellos CS, Duarte CA (2000) Hp-clouds in Mindlin's thick plate model. *Int J Numer Meth Eng* 47:1381–1400
8. Kanok-Nukulchai W, Barry W, Saran-Yasontorn K, Bouillard PH (2001) On elimination of shear locking in the element-free Galerkin method. *Int J Numer Meth Eng* 52:705–725
9. Krysl P, Belytschko T (1995) Analysis of thin plates by the element-free Galerkin method. *Comput Mech* 16:1–10
10. Krysl P, Belytschko T (1996) Analysis of thin shells by the element-free Galerkin method. *Inter J Solids Struct* 33:3057–3080
11. Liu WK, Jun S, Zhang YF (1995). Reproducing Kernel Particle Methods. *Int J Numer Meth Fluids* 20:1081–1106
12. Prathap G (1985) The curved beam/deep arch/finite ring element revisited. *Int J Numer Meth Eng* 21:389–407
13. Simo JC, Hughes TJR (1986), On the variational foundation of assumed strain method. *J Appl Mech* 53:51–54
14. Wang D (2003) Hybrid meshfree formulation for solids and structures. PhD dissertation, University of California, Los Angeles
15. Wang D, Chen JS (2004) Locking-free stabilized conforming nodal integration for meshfree Mindlin–Reissner plate formulation. *Comput Meth Appl Mech Eng* 193:1065–1083